Numerical Methods in Civil Engineering, 10-2 (2025) 27-43

Numerical Methods in Civil Engineering

Journal Homepage: https://nmce.kntu.ac.ir/

Flexural fatigue strength and failure probability of concrete beam containing nano-silica and steel fibers

Yaghoub Mohammadi*, Hassan Rezaei Dolagh**

ARTICLE INFO

RESEARCH PAPER

Article history:
Received:
October 2025
Revised:
December 2025
Accepted:
December 2025

Keywords:
Flexural fatigue,
Failure Probability,
Nano-silica,
Steel fibers,
Concrete beam

Abstract:

Roller-compacted concrete (RCC) shares components with conventional concrete but differs in aggregate size, workability, mix design, and construction methods. In pavements, repeated loading induces cracks that propagate over time, leading to fatigue failure. This study investigates improving the mechanical properties, flexural fatigue performance, and durability of RCC by incorporating nano-silica and steel fibers. Fatigue tests were conducted to evaluate 28-day flexural performance, and the number of cycles to failure at different stress levels was recorded. Fatigue-life data were analyzed using graphical methods, the method of moments, and maximum likelihood estimation to determine Weibull distribution parameters and hazard functions. Results demonstrate that adding nano-silica and steel fibers significantly enhances fatigue resistance, mechanical strength, and durability. Consequently, pavement thickness can be reduced, lowering both material usage and construction costs, while improving long-term performance. These findings highlight the effectiveness of nano-silica and steel fibers in producing more durable and cost-efficient RCC pavements.

1. Introduction

Continuous traffic loading, in concrete pavements, leads to the formation of cracks in critical sections, which grow over time. The growth of these cracks ultimately results in pavement failure due to fatigue. Fatigue can be viewed as progressive failure due to repetitive loadings, occurring at stress levels below the material's capacity [1].

Currently, the manufacturing of Portland cement accounts for 7% of carbon dioxide emissions each year, primarily resulting from clinker production [2]. Additionally, this process consumes a significant amount of energy and requires large quantities of raw materials. This has led the cement industry to be at odds with the principles of sustainable development [3]. Therefore, researchers are seeking suitable solutions to produce high-quality concrete to reduce the usage of natural raw resources and emissions of greenhouse gas [4].

The consumption of natural raw resources, low compressive strength at early ages, and environmental pollution are inherent drawbacks of conventional concrete [5]. Studies indicate that using concrete with reduced cement consumption leads to multiple benefits, such as decreased CO2 emissions and carbon-containing compounds, as well as the conservation of natural resources [6]. Population growth results in an exponential increase in construction activities worldwide, leading to a rise in demand for natural aggregates. The global demand for natural aggregates reached 40 billion tons in 2014, showing an average growth rate of about 8 percent. If the trend in the consumption of natural aggregates continues similarly, it can be assessed that the worldwide claim for natural aggregates will soon exceed 65 billion tons by 2022 [7, 8]. While it is impossible to halt the development of infrastructure and economic growth in countries, it is possible to strive for a balance between development and environmental issues by promoting sustainable, practical, and economical alternatives to existing materials. Paving with RCC is a modern innovation in construction, and its technology is advancing. The implementation of this type of paving has generally been favorable. RCC provides advantages like

* *Associate Professor, Department of Civil Engineering, University of Mohaghegh Ardabili, Ardabil, Iran. Email: yaghoubm@uma.ac.ir*
** *PhD Student, Department of Civil Engineering, University of Mohaghegh Ardabili, Ardabil, Iran. Email: rezaei.hassan@uma.ac.ir*

https://doi.org/10.61882/NMCE.2510.1103

lower expenses from its application technique and quicker execution times. RCC pavements do not utilize expansion joint reinforcement bars, reinforcing bars, or formwork. This results in considerable savings in comparison with typical concrete pavements. Besides, longitudinal and transverse shrinkage joints for crack control are usually not implemented in RCC pavements. Roller Compacted Concrete Pavement (RCCP) can be applied for several purposes, for instance, open areas of factories, access roads to mines, surfaces of port loading areas, heavy and military vehicle terminals, parking areas for cars and trucks, warehouse floors, aircraft parking areas at airports, low and medium-speed roads, and streets [9]. Research has shown that with an equal amount of cementitious materials, RCC exhibits higher compressive strength than typical concrete; on the other hand, the tensile strength is not necessarily greater than the typical one. Sufficient tensile strength is significant for preventing cracks caused by continuous loading or fatigue, particularly in pavements [10]. To achieve desirable physical properties in concrete, additives and reinforcement materials are incorporated into the concrete mix [11].

Researchers tested RCC using steel fibers of different sizes and amounts to see how they affect strength and workability. They found that increasing both the fiber content and fiber lenght improved the concrete's overall performance. However, the amount of fiber mattered more than the shape. The optimal outcomes were derived from using 0.75% of the longest fibers, hitting a sweet spot in strength and workability [12]. Different types of nano-materials improve the strength and durability of pavement-quality concrete (PQC), highlighting major boosts in performance. Nano SiO_2 and graphene oxide stood out, significantly enhancing key properties at low dosages. Nano TiO_2 also showed remarkable benefits, especially for abrasion and fatigue resistance [13]. Nano-silica enhances compressive strength and moisture resistance as well, while glass fibers significantly improve tensile strength and crack resistance [14].

Adding steel fibers and nano-silica improves the strength and performance of RCC pavement (RCCP). The highest performance was achieved by using 1% of both additives, boosting flexural strength by over 100% at 28 days. While strength improved significantly, workability decreased due to higher Vebe time and mix viscosity. Using these additives also allows for thinner pavements, saving materials, reducing weight, and speeding up construction [15].

Steel Fiber Reinforced Concrete (SFRC) is initially employed in the construction of slabs for pavements and industrial floors. Analysis of laboratory results from the U.S. Army Corps of Engineers Research Laboratory illustrated that beneath the same wheel load, SFRC slabs require approximately half the thickness of pure concrete slabs. The sustained functionality of the product is one of the greatest advantages of utilizing fiber reinforcement. Thereby, the crack control is one feature of functionality that can be improved through the use of fibers. Fibers can prevent the occurrence of wide cracks that lead to water infiltration and contamination. In addition to advantages such as crack control and serviceability, the tensile strength of the matrix can be expanded by employing fibers. Due to the flexibility of fiber-reinforced concrete construction methods, SFRC serves as a useful and economical structural material. The most important features of using SFRC include increased flexural stiffness, impact and fatigue resistance. Thus, SFRC is utilized in flat slabs subjected to heavy and impact loads [16].

Concrete fatigue under repeated loading must be carefully considered, as structural failure can occur even when induced stresses are below static strength. In pavements, fatigue cracking is a primary mode of failure. When a load passes over the pavement surface, horizontal compressive stresses develop in the upper portion, while tensile stresses arise in the lower portion. Repeated loading causes these stresses to accumulate, eventually resulting in fatigue cracks [17]. Researchers have extensively used various types of fibers with different properties in order to improve the fatigue life of typical concrete, and it has been shown that the use of fibers in typical concrete enhances fatigue performance [18, 19].

Accurately predicting pavement fatigue life is challenging due to complex interactions among loading, environmental conditions, and material properties. While traditional concrete pavements have been widely studied, roller-compacted concrete (RCC) has received limited attention, particularly regarding repeated loading. This study investigates the fatigue performance of RCC mixes modified with steel fibers and nano-silica to enhance durability and lifespan. Fatigue behavior is inherently random, so a probabilistic approach using the two-parameter Weibull distribution is applied. Distribution parameters are determined through graphical analysis, the method of moments, and maximum likelihood estimation. By modeling the fatigue performance of these modified RCC mixes, the study aims to quantify improvements in fatigue resistance. Incorporating steel fibers and nano-silica is expected to significantly strengthen RCC against repeated loading, offering practical insights for engineers and designers seeking to optimize pavement performance and longevity in real-world applications.

Because fatigue behavior in concrete is highly variable, engineers must rely on actual stress history and probabilistic tools to make informed decisions. By applying these statistical techniques, this study helps quantify the risk of premature failure and strengthens the foundation for more reliable pavement design [20]. A comprehensive

representation of fatigue data should encompass the relationship between the survival function $L_R(n)$, the distribution function $F_N(n)$, the applied stress S, and the fatigue life N.

Over the years, various mathematical models have been proposed to describe fatigue-life behavior, with the Weibull distribution, introduced by Weibull in 1939, becoming the most widely used due to its strong experimental basis and well-established statistical properties. This study emphasizes the statistical analysis of fatigue-life data using the Weibull distribution. Its fundamental characteristics are outlined, and methods for parameter determination graphical analysis, the method of moments, and maximum likelihood estimation are discussed and evaluated, demonstrating the applicability of the Weibull distribution for analyzing fatigue data.

Steel fibers and nano-silica particles are incorporated with the aim of overcoming the shortcomings of RCC and enhancing its mechanical properties, flexural fatigue performance, and overall durability in pavement applications. The study thoroughly investigates the influence of these additives on improving the behavior of RCC.

2. Weibull Distribution

In fatigue design, several key factors, such as material strength and loading conditions, are treated as statistical variables due to their natural variability. On top of that, uncertainties also stem from the assumptions adopted in the analysis, as well as the unpredictable nature of construction materials themselves. Together, these factors make a probabilistic approach essential for reliable fatigue design. Designers must reflect the uncertainties in fatigue behavior in the design stresses to ensure adequate fatigue resistance. Probabilistic reliability theory is an effective method for calculating these types of uncertainties.

Various mathematical models have been illustrated in order to describe fatigue data statistically. According to the ASTM standards, fatigue life (N) should be treated as normally distributed based on the recommendations [21]. The log-normal distribution function has also been widely used. The acceptance of the log-normal distribution was initially based on the convenience of mathematical application. For a log-normal distribution, the hazard function falls off as the number of cycles rises [22]. Based on correct physical assumptions, laboratory validation, relative ease of application, and more appropriate statistical development, the Weibull distribution is employed to explain fatigue data statistically [23].

The Weibull function takes the following form: (the f(n) and $F_N(n)$ express the probability and the cumulative distribution function, respectively) [24].

$$f(n) = \frac{\alpha}{u - n_0}\left[\frac{n - n_0}{u - n_0}\right]^{\alpha - 1} exp\left[-\left(\frac{n - n_0}{u - n_0}\right)^{\alpha}\right] \quad (1)$$

$$F_N(n) = 1 - exp\left[-\left(\frac{n - n_0}{u - n_0}\right)^{\alpha}\right] \quad (2)$$

For $\geq n_0 : \alpha > 0:\ u > n_0$

Where

n is the random variable of N

α is the Weibull slope or shape parameter at the stress level

u is the scale parameter at the stress level

n_0 is the minimum lifespan or parameter at the stress level

A physical assumption where the hazard function increases with time leads to a Weibull distribution [25]. The hazard function $H_z(n)$ of the Weibull distribution can be written as follows [26]:

$$H_z(n) = \frac{\alpha}{u - n_0}\left[\frac{n - n_0}{u - n_0}\right]^{\alpha - 1} \quad (3)$$

The hazard function increases with the increase of the shape parameter α > 1.0 [27], which corresponds to the anticipated fatigue behavior of the material. For instance, in an erosive process such as fatigue, the hazard function $H_z(n)$ increases with cumulative irreversible microstructural failure [28].

The hazard function of the Weibull distribution can be represented in various forms based on the parameter α. The survival function or probability of survival or reliability function, $L_R(n)$, is represented by the following:

$$L_R(n) = 1 - F_N(n) \quad (4)$$

By substituting the value of $F_N(n)$ from equation (2) into equation (4):

$$L_R(n) = exp\left[-\left(\frac{n - n_0}{u - n_0}\right)^{\alpha}\right] \quad (5)$$

In fatigue, it is logical to assume that the minimum life is equal to $n_0 = 0$, then equation (5) can be expressed as below:

$$L_R(n) = exp\left[-\left(\frac{n}{u}\right)^{\alpha}\right] \quad (6)$$

Equation (6) is defined as the two-parameter Weibull distribution. Although the distribution function is commonly preferred, this study employs the survival function due to its simpler form. The two-parameter Weibull distribution is widely recognized for modeling the fatigue behavior of engineering materials, owing to its greater reliability. Additionally, statistical analysis methods for the Weibull distribution have been suitably developed. Some characteristics of the Weibull distribution used in fatigue testing are as follows:

The variable N, a random variable that indicates the number of cycles before sample failure, is labeled as n_0 for $n > n_0$. Therefore, n_0 represents the minimum fatigue life, and

$L_R(n_0) = 1$, meaning that no failure can occur in less than n_0 cycles.
When $n =$ u

$$L_R(u) = \frac{1}{e} = 0.368 \quad (7)$$

Equation (7) is used to determine the u parameter. In the three-parameter Weibull distribution, α, u, and n_0 are functions of S, while in the two-parameter distribution ($n_0 = 0$), α is constant.
Different forms of the probability density function are obtained by using various values of the shape parameter α. For values of α equal to 1 and 2, the Weibull distribution transforms into the exponential distribution and the Rayleigh distribution, respectively. At $\alpha = 3.57$, the shape of the Weibull distribution becomes the normal distribution [21, 29].
Several methods have been proposed for determining the shape parameter α and the scale parameter u in the two-parameter Weibull survival function. Three methods, namely 1) graphical method, 2) moment method, and 3) maximum likelihood method, have been introduced and explained. It is worth mentioning that assuming a minimum fatigue life of $n_0 = 0$ results in a more conventional model:

$$L_R(n) = 1 - F_N(n) = exp\left[-\left(\frac{n}{u}\right)^{\alpha}\right] \quad (8)$$

2.1 Graphical Method

By taking the logarithm of both sides of Equation (8), it is obtained:

$$\ln L_R = -\left(\frac{n}{u}\right)^{\alpha} \quad (9)$$

The logarithm is taken from both sides of equation (9) again:

$$\ln\left[\ln\left(\frac{1}{L_R}\right)\right] = \alpha \ln(n) - \alpha \ln(u) \quad (10)$$

Equation (10) can be written as follows:

$$Y = \alpha X - B$$

Where

$$Y = \ln\left[\ln\left(\frac{1}{L_R}\right)\right] \qquad X = \ln(n) \qquad B = \alpha \ln(u)$$

Equation (10) shows a linear relationship between Y and X. The fatigue life data at a specific stress level are arranged in descending order based on the number of cycles to failure. The empirical survival function, L_R, for fatigue life data at a given stress level is determined using the following equation [30]:

$$L_R = 1 - \frac{i}{k+1} \quad (11)$$

i and k illustrate the sample order number and fatigue data number at a specific stress level, respectively.
The chart displays a plot of $\ln\left[\ln\left(\frac{1}{L_R}\right)\right]$ versus $\ln(N)$. A regression analysis is used to draw a line which fits the whole plotted data, similar to the least squares method. The slope of the line represents the shape parameter α, and the characteristic life u is determined through the value of N at $L_R = 0.368$ or $F = 63.20\%$ according to equation (7).
Figure 1 provides a schematic illustration of how the parameters of the two-parameter Weibull distribution are determined.

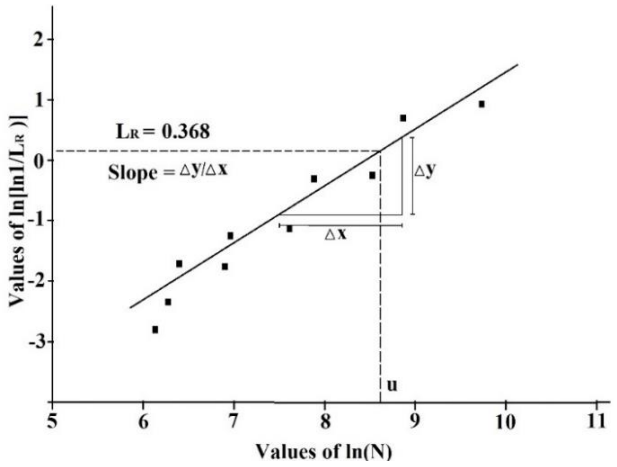

Fig. 1: Determination of Weibull distribution parameters using graphical method

2.2 Moment Method

To estimate the Weibull distribution parameters (α and u), reliable calculations of the sample's average and variability are required. The general form of the Weibull distribution can be expressed as follows:

$$E[(N - n_0)^c] = Y_0^c \Gamma\left(\frac{C}{\alpha} + 1\right) \quad (12)$$

E represents mathematical hope; $Y_0 = u - n_0$; $\Gamma(x)$ is defined as the gamma function, and C is a constant number. If $n_0 = 0$, equation (12) becomes as follows:

$$E(N^C) = Y^C \Gamma\left(\frac{C}{\alpha} + 1\right) \quad (13)$$

If C=1 and C=2, then:

$$E(N) = Y\Gamma\left(\frac{1}{\alpha} + 1\right) \quad (14)$$

$$E(N^2) = Y^2 \Gamma\left(\frac{2}{\alpha} + 1\right) \quad (15)$$

Considering that $\mu = E(N)$ and $\sigma^2 = E(N^2) - \mu^2$ are the mean and variance of the data at stress level S, which are determined by equations (14) and (15), they can be expressed as follows:

$$\frac{\alpha}{\mu}=\left[\frac{\Gamma\left(\frac{2}{\alpha}+1\right)}{\Gamma^2\left(\frac{1}{\alpha}+1\right)}-1\right]^{\frac{1}{2}} \quad (16)$$

Due to the difficulty in determining the parameter α from equation (16), the value of α can be approximately estimated using the following expression [25]:

$$\alpha=(CV)^{-1.08} \quad (17)$$

The lifespan characteristic u can be determined from equation (14) by substituting μ into $E(N)$ as follows:

$$u=\frac{\mu}{\Gamma\left(\frac{1}{\alpha}+1\right)} \quad (18)$$

2.3 Maximum Likelihood Method

The probability density function of the Weibull distribution (Equation (1)) is represented by the following:

$$f_N(n)=\frac{\alpha}{\Theta}n^{\alpha-1}\exp\left[-\frac{n^\alpha}{\Theta}\right] \quad (19)$$

Where

$$\Theta=u^\alpha \quad (20)$$

Therefore, the probability function takes the following form [31]:

$$L(\alpha,\Theta\,|n_1,n_2,\dots,n_k)=\prod_{i=1}^{k}f(ni|\alpha,\Theta) \quad (21)$$

Equation (21) can be expressed in logarithmic form as follows:

$$\begin{aligned}\ln\left(L(\alpha,\Theta\,|n_1,n_2,\dots,n_k)\right)&=ln\left[\prod_{i=1}^{k}f(ni|\alpha,\Theta)\right]\\&=\sum_{i=1}^{k}ln[f(ni|\alpha,\Theta)]\end{aligned} \quad (22)$$

We differentiate equation (22) with respect to α and Θ, set it equal to zero, and solve the resulting equations for α and Θ, which leads to the following equations:

$$\Theta^*=\frac{1}{k}\sum_{i=1}^{k}{n_i}^{\alpha^*} \quad (23)$$

$$\frac{\sum_{i=1}^{k}{n_i}^{\alpha^*}\ln(n_i)}{\sum_{i=1}^{k}{n_i}^{\alpha^*}}-\frac{1}{\alpha^*}=\frac{1}{k}\sum_{i=1}^{k}\ln(n_i) \quad (24)$$

Such that α^* and $\Theta^*$are the maximum likelihood estimators of α and Θ, respectively. The parameter α can be calculated from equation (24) and an iterative computer program. Then, the parameter u is defined by the expression $u=\Theta^{\frac{1}{\alpha}}$ (Equation (20)).

3. Materials Used

When selecting the type of materials for use in RCC mixes, design strength, durability requirements, and the type of application are influential factors. The main materials used in the production of RCC include water, cementitious materials, and fine and coarse aggregates [32]. Additionally, nano-silica and steel fibers have been used to create RCC composites.

3.1 Cement

The cement utilized is the pozzolanic Portland cement type produced at the Arta Ardabil Cement Factory, which complies with the ASTM C595-79 standard [33].
The physical and chemical specifications of the cement are presented in Table 1, and images taken using an electron microscope are shown in Figure 2.

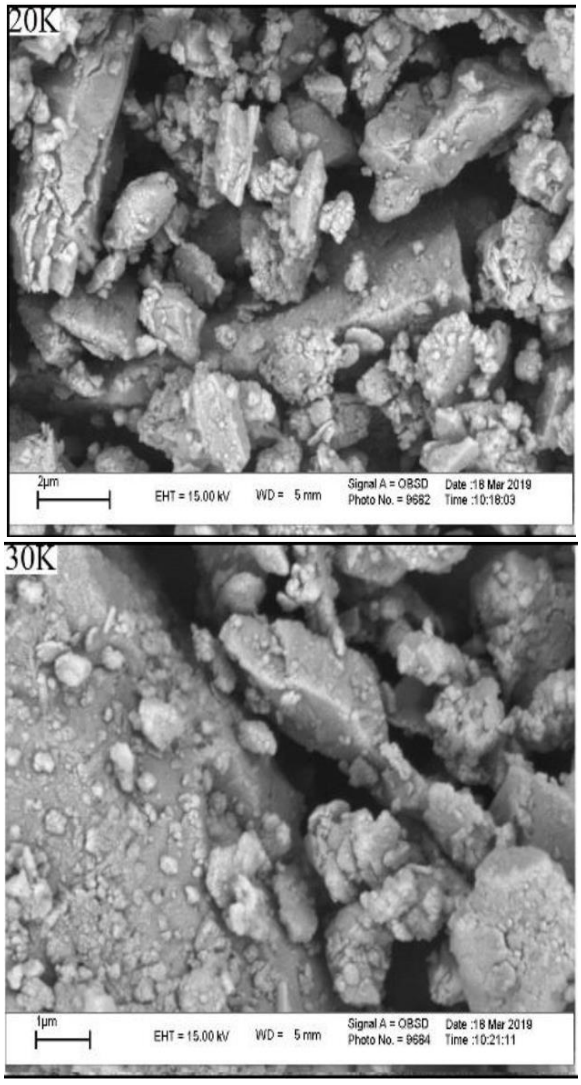

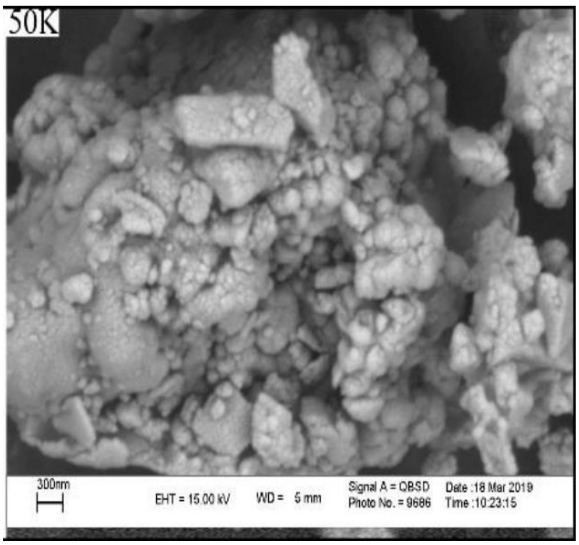

Fig. 2: SEM images of cement particles at magnifications of 20,000, 30,000, and 50,000 times

Table 1: Chemical Composition and Physical Properties of the Cement Used

Cement	Chemical Composition(%)
20.95	SiO_2
4.98	Al_2O_3
4.09	Fe_2O_3
63.21	CaO
1.37	MgO
2.27	SO_3
0.48	Na_2O
0.78	K_2O
-	TiO_2
-	MnO
-	P_2O_5
1.65	Loss of Inertness
35-60	C_3S
20-35	C_2S
9-11	C_3A
9-12	C_4AF
-	Physical Specifications
16.00 µm	Particle dimensions
3.13	Density(g/cm^3)
0.300	Specific surface area (m^2/g)

3.2 Nano-silica

The nano-silica used is in powdered form and produced by the Aerosil Company. This material is utilized as a partial replacement for the cement used, based on a percentage of weight in RCC mixtures. The appearance of the nano-silica used, with an average particle size of 10 to 20 nanometers, is presented in the images obtained using an electron microscope in Figures 3 and 4.

Fig. 3: Powdered nano-silica used

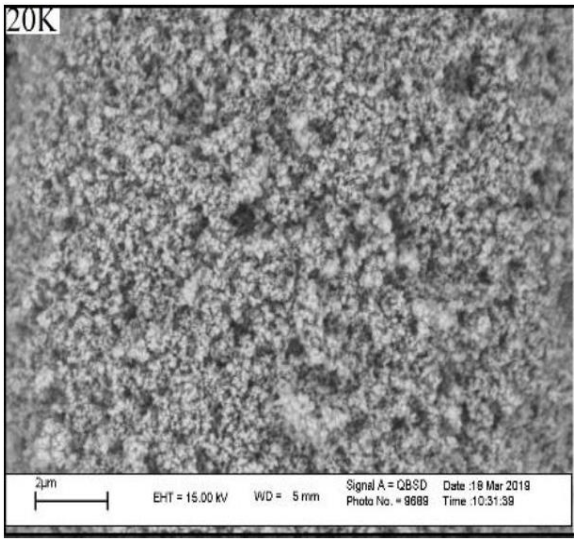

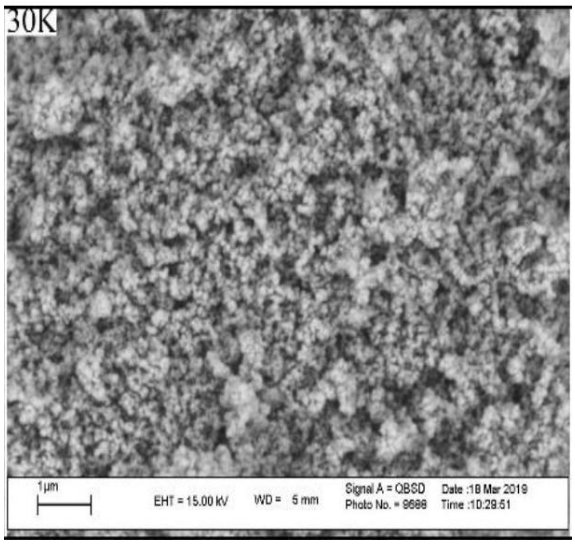

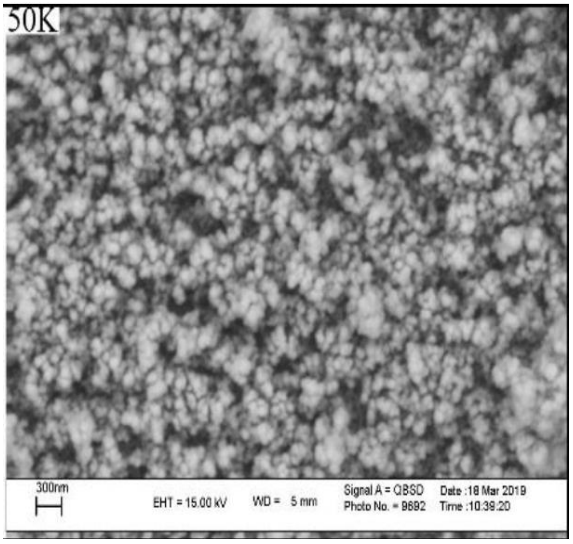

Fig. 4: SEM images of nano-silica particles at magnifications of 20,000, 30,000, and 50,000 times

3.3 Water

The quality of water for RCC pavement is similar to that of ordinary concrete [32]. The water used for mixing and curing all samples is drinking water from Ardabil City, which meets the recommended standards of ASTM D1129 [34]. Since this water has no specific taste or odor and is potable, it can be used for the production of RCC.

3.4 Aggregates

The aggregates, sand and gravel, extracted from the village of Gilehdeh in Astara, are studied. The coarse aggregates are of the crushed type with a maximum nominal size of 12.8 mm. In this study, the grading was conducted according to ASTM C136 [35]. The aggregates grading is provided in Table 2, which complies with the grading suggested by ACI 325.10R [9] for use in roller compacted concrete. The bulk density was defined based on ASTM C29 [36], while the specific gravity and water absorption of both fine and coarse aggregates were determined following the ASTM C128 and C127 standards. The physical properties of the aggregates used are presented in Table 3.

This study aims to investigate the effect of using nano-silica and steel fibers on the properties of roller compacted concrete composites.

3.5 Steel Fibers

In this study, steel fibers with a circular cross-section (Figure 5) and physical specifications listed in Table 4, produced by Durochem Company in Italy, were utilized. Steel fibers were used in RCC mixtures based on a percentage of the volume of the concrete.

Table 2: Analysis of the Gradation of Used Aggregates

Passing Percentage Used Aggregate (%)	ACI 325.10R		Screen Size	Screen NO
	Max	Min		
		100	25 mm	1 in
100	100	84	19 mm	3/4 in
79	86	66	9.5 mm	3/8 in
62	69	51	4.75 mm	NO.4
41	56	38	2.36 mm	NO.8
31	47	28	1.18 mm	NO.16
20	37	18	600 µm	NO.30
15	27	12	300 µm	NO.50
7	18	6	150 µm	NO.100
2	8	2	75 µm	NO.200

Table 3: Physical Specifications of the Sand and Gravel Used

Specifications	Fine aggregates	Coarse aggregates
specific gravity (gr/cm^3)	2.64	2.69
Bulk specific gravity (kg/m^3)	-	16000
Water absorption (%)	5.0	1.3
Fineness modulus	3.0	-

Table 4: Specifications of Used Steel Fibers

Specifications	Steel Fibers
Length(mm)	50
Diameter(mm)	0.8
Average apparent ratio(l/d)	62.5
Tensile strength (MPa)	1000
elasticity Modulus(GPa)	200
specific gravity	7.85

Fig. 5: Steel fibers used

4. Roller Compacted Concrete Mix Design

Two main methods are used to determine RCC mixing ratios. The first targets low-cement mixes with coarse aggregates (maximum size ≥37.5 mm) for mass concrete, focusing on workability. The second applies to thin layers like pavements, based on soil compaction. Both ensure sufficient paste to fill voids between aggregates and properly coat the particles [16].

A custom RCC mix was developed through material testing and evaluation of key requirements, aiming for strong and workable concrete. The study also examined the effects of nano-silica and steel fibers, using hands-on testing due to the absence of fixed RCC mix design standards.

The mix design for conventional paving concrete was carried out according to ACI 211.1 [37], while the mix design for roller-compacted paving concrete followed ACI 211.3R. The average compressive strength required for paving concrete is typically considered to be 30 MPa. Additionally, the slump value for conventional paving concrete is estimated to be between 25 mm and 75 mm [38]. This study is planned in four sections. In the first stage, five mix designs for pure RCC (without nano-silica and steel fibers) were developed within a compressive strength range of 20 MPa to 40 MPa (Table 5). The naming convention is as follows: the letter P indicates the purity of the RCC (lacking nano-silica and steel fibers), the number represents the mix number, and RCC denotes RCC. For each mix design, 27 samples were created (18 cylindrical samples and 9 beam samples), totaling 135 samples for testing tensile, flexural, and compressive strengths at 7, 28, and 90 days.

Table 5: Mix Designs for Pure RCC.

Mixing NO	Mixing Name	Slump (mm)	Coarse aggregates(kg)	Fine aggregates(kg)	Cement (kg)	Water (kg)
1	P1RCC	0	1371	530	307	171
2	P2RCC	0	1442	466	311	168
3	P3RCC	0	1405	480	320	177
4	P4RCC	0	1326	528	347	185
5	P5RCC	0	1305	526	360	193

From each mix design, 27 samples were prepared (18 cylindrical samples and 9 beam samples), totaling 405 samples for compressive, tensile, and flexural strength tests at 7, 28, and 90 days. In the third stage, cubic samples were created for 20 mix designs from the first and second stages (5 pure roller concrete mix designs and 15 composite roller concrete mix designs), resulting in a total of 60 samples subjected to 28-day permeability testing. In the fourth stage, beam samples were produced for 15 mix designs from the first and second stages (4 pure roller concrete mix designs and 11 composite roller concrete mix designs), with 30 samples for each mix design at different stress levels of 0.95, 0.90, and 0.85, totaling 450 samples tested for fatigue. Nano-silica was incorporated at dosages of 0.5%, 1.0%, and 1.5% by weight of cement, were added at volume fractions of 0.33%, 0.67%, and 1.00% by volume of concrete. The mixing ratios are presented in Table 6.

In the second phase, 15 mix designs for RCC composites containing nano-silica and steel fibers have been considered. The naming convention is as follows: the letter C indicates the composite (containing either nano-silica or steel fibers), the number denotes the mix number, RCC signifies RCC, the first subscript indicates the weight percentage of nano-silica relative to the weight of cement, and the second subscript indicates the percentage of steel fibers relative to the volume of concrete.

Among the designed pure RCC mixes, P1RCC has a compressive strength of 22.64 MPa, which is lower than the recommended minimum compressive strength of 27.6 MPa for RCC pavement. In contrast, P2RCC has a compressive strength of 25.57 MPa, which is close to the compressive strength recommended by ACI 325.10R. Therefore, this mix design (P2RCC) was used as the base mix for constructing RCC composites for pavement in this research.

4.1 Preparation of RCC Specimens

Based on the mix design, coarse aggregate, sand, water, cement, nano-silica, and steel fibers were prepared in specified amounts. The powdered nano-silica was first dispersed in one-third of the mixing water using a mechanical mixer. The mixing sequence involved adding coarse aggregate and part of the water, followed by sand with additional water, then cement and the nano-silica solution, and finally steel fibers with the remaining water to ensure uniform distribution. The mixture was then mechanically mixed for 3 minutes, rested for 3 minutes, and mixed again for 2 minutes.

To prevent segregation and ensure homogeneity, the concrete was further hand-mixed before being placed into molds on a vibrating table with a surcharge applied. Vibration continued until the mortar filled the annular space around the surcharge. Cylindrical specimens were cast in three layers, while prismatic beams were cast in a single layer. All casting was completed within 45 minutes of mixing, and no super-plasticizers were used to avoid potential interactions with nano-silica.

Table 6: Mix Designs of Roller Compacted Concrete Composites

Mixing NO	Mixing Name	Slump (mm)	Coarse aggregates (kg)	Fine aggregates (kg)	Cement (kg)	Water (kg)	Steel fibers (kg)	Nano –silica (kg)
0	P2RCC	٠	1442	466	311	168	00.0	0.000
1	$C1RCC_{0.0\text{-}0.33}$	٠	1442	466	311	168	25.9	0.000
2	$C2RCC_{0.0\text{-}.0.67}$	٠	1442	466	311	168	51.8	0.000
3	$C3RCC_{0.0\text{-}1.00}$	٠	1442	466	311	168	78.5	0.000
4	$C4RCC_{0.5\text{-}0.00}$	٠	1442	466	311	168	00.0	1.555
5	$C5RCC_{0.5\text{-}0.33}$	٠	1442	466	311	168	25.9	1.555
6	$C6RCC_{0.5\text{-}0.67}$	٠	1442	466	311	168	51.8	1.555
7	$C7RCC_{0.5\text{-}1.00}$	٠	1442	466	311	168	78.5	1.555
8	$C8RCC_{1.0\text{-}0.00}$	٠	1442	466	311	168	00.0	3.110
9	$C9RCC_{1.0\text{-}0.33}$	٠	1442	466	311	168	25.9	3.110
10	$C10RCC_{1.0\text{-}0.67}$	٠	1442	466	311	168	51.8	3.110
11	$C11RCC_{1.0\text{-}1.00}$	٠	1442	466	311	168	78.5	3.110
12	$C12RCC_{1.5\text{-}0.00}$	٠	1442	466	311	168	00.0	4.665
13	$C13RCC_{1.5\text{-}0.33}$	٠	1442	466	311	168	25.9	4.665
14	$C14RCC_{1.5\text{-}0.67}$	٠	1442	466	311	168	51.8	4.665
15	$C15RCC_{1.5\text{-}1.00}$	٠	1442	466	311	168	78.5	4.665

4.2 Compaction of RCC Mixtures

Since RCC mixtures are slump-free, conventional concrete specimen preparation methods cannot be directly applied for fabricating RCC samples. Commonly employed techniques include vibrating the fresh RCC specimen on a vibration table under a static load according to ASTM C1176 [39] or compacting the specimen using a vibratory hammer as per ASTM C1435 [40].

Both the vibratory hammer and the loaded vibration table can be utilized for compacting cylindrical specimens. However, for beam specimens with large surface areas or for cubic samples, compaction using a vibratory hammer is impractical, and static-load vibration compaction is more suitable [16]. Slump-free concrete must be mixed using a mechanical mixer, with spiral and pan mixers proving more effective than conventional mixers for such mixes [41]. In this study, a vibration table under a static load of 1.9 kg was employed to prepare cylindrical specimens measuring 150 × 300 mm, in accordance with ASTM C1176, ACI 215R and fib Model Code 2010.

Since no specific standard exists for fabricating beam specimens of 100 × 100 × 350 mm and cubic specimens of 150 × 150 × 150 mm, a vibration table was used. The static load was adjusted to match the contact pressure of the respective beam specimens, resulting in weights of 6 kg and 8.5 kg, respectively (Figure 6).

Fig. 6: Compaction of cylindrical and beam specimens using a vibration table with static load

4.3 Specimen Casting

After completing the slump-flow test, all mixtures were cast into molds for hardened concrete testing. The specimen dimensions considered in the present study are as follows:

1. Cylindrical specimens (150 × 300 mm): These specimens were used to determine the compressive strength and indirect tensile strength (Brazilian splitting test) of the roller-compacted concrete mixtures.
2. Prismatic (beam) specimens (100 × 100 × 350 mm): These specimens were used to evaluate the flexural strength, flexural toughness, and fatigue behavior of the roller-compacted concrete mixtures.
3. Cubic specimens (150 × 150 × 150 mm): These specimens were employed to assess water permeability in concrete (Figure 7).

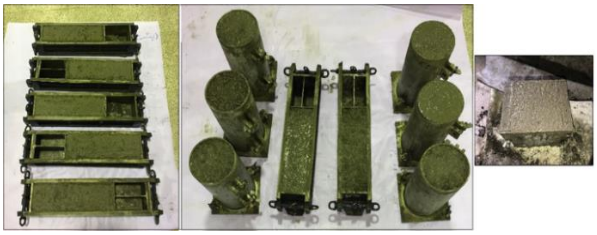

Fig. 7: Casting of Cylindrical, Beam, and Cubic specimens

4.4 Specimen Curing

After casting the mixtures under investigation, all specimen surfaces were covered with plastic sheets to prevent moisture evaporation and left undisturbed for 24 hours. After this initial period, the molds were removed, and the specimens were cured in a water tank maintained at 23 ± 2°C. Upon completion of the designated curing period, the specimens were taken out of the water and prepared for testing (Figure 8) [42].

Fig. 8: Specimen curing

5. Flexural Fatigue Tests

Concrete can gradually weaken under repeated loading, even when the applied stress levels are below its monotonic strength capacity. That's why this study looked at how RCC (RCC) performs under bending fatigue, especially when reinforced with steel fibers. These fibers enhance strength and fatigue resistance, but their impact varies depending on their shape, size, texture, and their distributed within the mix.

From 20 concrete mix variations, 15 were chosen for testing. First, their basic bending strength was measured, which was then used to set the range for fatigue testing. The samples were exposed to repeated, wave-like loads until they failed, and the number of cycles each one survived was recorded as its fatigue life.

To keep testing practical while still gathering reliable results, 10 samples were tested at each stress level. All samples were 28 days old to ensure consistency, and beam-shaped specimens were used under controlled loading conditions.

Fatigue is commonly characterized by a parameter referred to as fatigue life, which is the number of cycles required until the material fails under a specified repeated loading. In this study, flexural fatigue tests are organized into a fixed stress ratio ($R=f_{min}/f_{max}$) of 0.1 and varying stress levels ($S=f_{max}/f_r$) of 0.95, 0.90, and 0.85.

A proportion of the modulus of rupture, representing the stress level, is utilized for fatigue testing. The maximum fatigue stress (f_{max}) applied to the specimens during the fatigue test is derived from the final static fatigue stress (f_r), which is obtained through static bending tests. Subsequently, the minimum fatigue stress (f_{min}) applied to the specimen is calculated for each specified stress ratio ($R=f_{min}/f_{max}$), using the previously determined maximum fatigue stress (f_{max}). The corresponding minimum and maximum fatigue loads (P_{max} and P_{min}) are then determined based on the minimum and maximum static bending resistances. The defined stress level and stress ratio are subsequently converted into their respective equivalent fatigue loads (P_{max}, P_{min}). The obtained minimum and maximum fatigue loads are applied iteratively to the beam sample until failure occurs. A sample of the calculations for determining the maximum and minimum fatigue loads is shown in Table 7.

$$P_{max} = \frac{(f_{max})bh^2}{L} \tag{25}$$

$$P_{min} = \frac{(f_{min})bh^2}{L} \tag{26}$$

Similar to static bending tests, the samples are placed perpendicularly to the molding direction on the supports. The fatigue test is conducted between the two maximum and minimum load limits that have been calculated. A constant amplitude load is applied to the sample in a sinusoidal manner at a frequency of 1.4 Hz. Therefore, this test can be considered a low-cycle fatigue test [32]. The schematic configuration of the flexural fatigue test is depicted in Figure 9, while the applied fatigue loading protocol is illustrated in Figure 10. For pure RCC samples and RCC composites containing steel fibers and nano-silica particles at volume ratios of 0.33, 0.67, and 1 percent, and weight ratios of 0.5 and 1 percent, the number of cycles to failure for each specified stress level was recorded. As the stress levels decrease, the number of cycles to sample failure increases.

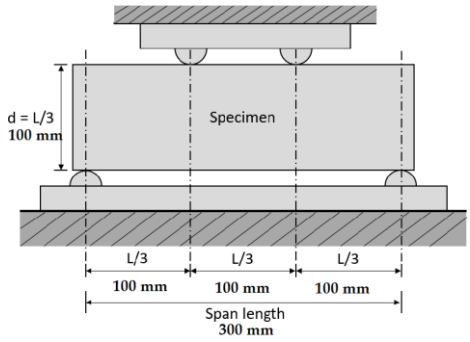

Fig. 9: Schematic diagram of the bending fatigue test

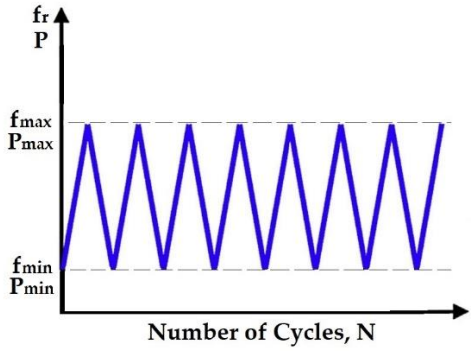

Fig. 10: Applied fatigue loading schematic

Table 7: Sample Calculations for Determining Minimum and Maximum Fatigue Loads

Static Flexural Stress, f_r (MPa)	5
Stress Level $S=f_{max}/f_r$	0.95
Max. Fatigue Stress, $f_{max}=S\times f_r$ (MPa)	4.75
Stress Ratio $R=f_{min}/f_{max}$	0.1
Min. Fatigue Stress, $f_{min}=R\times f_{max}$ (MPa)	0.475
Max. Fatigue Load, P_{max}(kN)	15.833
Min. Fatigue Load, P_{min}(kN	1.583

To explore how RCC (RCC) behaves under repeated stress, three different analysis methods were used to study its fatigue life at various stress levels. Tests were carried out on both plain RCC and mixes improved with steel fibers and nano-silica in different amounts.

At higher stress, the concrete failed quickly after the first crack appeared. At lower stress, it managed to keep going for more cycles, even with visible cracks.

6. Flexural Fatigue Test Results

6.1 Fatigue-Life Distribution of Plain and RCC Composite

The analytical procedures used to evaluate fatigue-life distribution at different stress levels together with the determination of the shape parameter (α) and the life characteristic (u) of the two-parameter Weibull distribution are presented in detail in Chapter 8.

These procedures, including the graphical method, the method of moments, and the maximum likelihood estimation method, were applied to assess the fatigue-life distribution of plain RCC and RCC composites containing steel fibers and nano-silica at stress levels of 0.95, 0.90, and 0.85. The composite mixtures incorporated steel fibers at volume fractions of 0.33%, 0.67%, and 1.00%, as well as nano-silica at weight contents of 0.5%, 1.0%, and 1.5%.

At higher stress levels, failure occurred immediately after the first visible crack appeared. In contrast, at lower stress levels, the specimens were able to withstand a significantly larger number of load cycles even after the onset of initial cracking. In the RCC composite specimens, failure was attributed partly to fiber pull-out and partly to the rupture of individual fibers. As the number of cycles increased and cracks propagated, audible sound from fiber breakage could be detected.

6.2 Analysis Using the Graphical Method

To analyse how fatigue life is distributed under different stress levels, a graphical method was applied to both plain RCC and mixes enhanced with steel fibers and nano-silica. The fiber content was varied at volume ratios of 0.33%, 0.67%, and 1%, while nano-silica was added at weight ratios of 0.5%, 1%, and 1.5%. Correlation values and Weibull parameters for each stress level are detailed in Table 8 and depicted in Figure 11.

The two-parameter Weibull distribution was used to interpret and represent the results. Table 9 shows the calculations related to the plotting of fatigue life data at different stress levels of 0.95, 0.90, and 0.85 for pure roller compacted concrete**.**

Table 8: Weibull distribution parameters at different stress levels of P4RCC roller compacted concrete samples

	Parameter	Stress Level (S)		
		0.95	0.9	0.85
P4RCC	α	2.3392	2.1632	1.8605
	B	6.7008	9.4676	10.8420
	u	17.5414	79.5719	339.4959

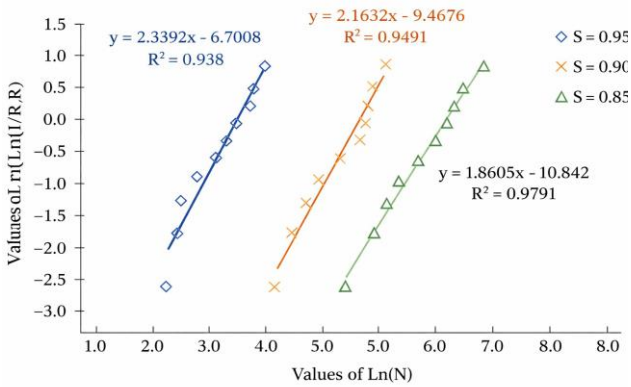

Fig. 11: Graphical Analysis of Fatigue-Life Data at Various Stress Levels for P4RCC RCC Specimens

Table 9: Data on fatigue life and empirical survival function at different stress levels of P4RCC RCC samples

P4RCC						
Stress Level (S)	**i**	**N_i**	**L_R**	**Ln(Ln(1/L_R))**	**Ln(N)**	**F=1-L_R**
0.95	1	8	0.9091	-2.3506	2.0794	0.0909
	2	9	0.8182	-1.6061	2.1972	0.1818
	3	9	0.7273	-1.1443	2.1972	0.2727
	4	11	0.6364	-0.7941	2.3979	0.3636
	5	14	0.5455	-0.5007	2.6391	0.4545
	6	16	0.4545	-0.2377	2.7726	0.5455
	7	18	0.3636	0.0115	2.8904	0.6364
	8	21	0.2727	0.2618	3.0445	0.7273
	9	22	0.1818	0.5334	3.0910	0.8182
	10	25	0.0909	0.8746	3.2189	0.9091
0.9	1	31	0.9091	-2.3506	3.4340	0.0909
	2	36	0.8182	-1.6061	3.5835	0.1818
	3	42	0.7273	-1.1443	3.7377	0.2727
	4	49	0.6364	-0.7941	3.8918	0.3636
	5	66	0.5455	-0.5007	4.1897	0.4545
	6	83	0.4545	-0.2377	4.4188	0.5455
	7	88	0.3636	0.0115	4.4773	0.6364
	8	91	0.2727	0.2618	4.5109	0.7273
	9	94	0.1818	0.5334	4.5433	0.8182
	10	109	0.0909	0.8746	4.6913	0.9091
0.85	1	108	0.9091	-2.3506	4.6821	0.0909
	2	148	0.8182	-1.6061	4.9972	0.1818
	3	166	0.7273	-1.1443	4.1120	0.2727
	4	193	0.6364	-0.7941	4.2627	0.3636
	5	256	0.5455	-0.5007	5.5452	0.4545
	6	318	0.4545	-0.2377	5.7621	0.5455
	7	359	0.3636	0.0115	5.8833	0.6364
	8	387	0.2727	0.2618	5.9584	0.7273
	9	433	0.1818	0.5334	6.0707	0.8182

6.3 Average Parameters of the Two-Parameter Weibull Distribution for Fatigue-Life Data at Different Stress Levels

The fatigue-life data obtained at various stress levels were analyzed using three statistical approaches graphical fitting, the method of moments, and maximum likelihood estimation to characterize their conformity to the two-parameter Weibull distribution. The results for plain RCC and RCC composites reinforced with steel fibers and nano-silica are reported in Tables 10 and 11. The composites include steel fibers at volumetric ratios of 0.33%, 0.67%, and 1%, and nano-silica at weight fractions of 0.5%, 1%, and 1.5%.

7. Maximum Load

The maximum load values of the 28-day specimens for both plain RCC and RCC composites incorporating steel fibers and nano-silica at volumetric fiber contents of 0.33%, 0.67%, and 1%, and nano-silica contents of 0.5%, 1%, and 1.5% by weight are presented in Table 12. A comparison of these results is illustrated in Figure 12. The P2RCC mixture is considered the control sample.

Table 10: Average Parameters of the Weibull Distribution for Fatigue-Life Data at Various Stress Levels of P4RCC

		Estimated Parameters	Stress Level (S)		
			0.95	0.9	0.85
P4RCC	Graphical Method	α	2.3392	2.1632	1.8605
		u	17.5414	79.5719	339.4959
	Method of Moments	α	2.7118	2.6689	2.12932
		u	17.2022	77.5081	331.4023
	Maximum Likelihood	α	2.9447	2.9664	2.2999
		u	17.2227	77.5684	334.6612
	Average	α	2.6652	2.5995	2.0966
		u	17.3221	78.2161	335.1865

Table 11: Average Parameters of the Weibull Distribution for Fatigue-Life Data at Various Stress Levels of RCC Composite Specimens

		Estimated Parameters	Stress Level (S)		
			0.95	0.9	0.85
C5RCC$_{0.5\text{-}0.33}$	Graphical Method	α	3.1529	2.7573	2.3301
		u	19.8304	85.6582	343.3491
	Method of Moments	α	3.6218	3.3079	2.5282
		u	19.6361	84.2693	337.3459
	Maximum Likelihood	α	3.8678	3.6224	2.7276
		u	19.6065	84.1427	339.1900
	Average	α	3.5475	3.2292	2.4953
		u	19.6910	84.6900	339.9617

Table 12: Average Maximum load of 28-day pure RCC and RCC composite specimens and comparison with the control mix.

Percentage change	Average maximum load (N)	Mix designation
-6.7	15555.6	P1RCC
0.0	16666.7	P2RCC
7.6	17933.3	P3RCC
21.2	20200.0	P4RCC
28.1	21355.6	P5RCC
10.2	18366.7	C1RCC$_{0.0\text{-}0.33}$
58.0	26333.3	C2RCC$_{0.0\text{-}.0.67}$
87.2	31200.0	C3RCC$_{0.0\text{-}1.00}$
2.6	17100.0	C4RCC$_{0.5\text{-}0.00}$
11.0	18500.0	C5RCC$_{0.5\text{-}0.33}$
59.2	26533.3	C6RCC$_{0.5\text{-}0.67}$
99.2	33200.0	C7RCC$_{0.5\text{-}1.00}$
8.8	18133.3	C8RCC$_{1.0\text{-}0.00}$
14.2	19033.3	C9RCC$_{1.0\text{-}0.33}$
72.2	28700.0	C10RCC$_{1.0\text{-}0.67}$
102.6	33766.7	C11RCC$_{1.0\text{-}1.00}$
-15.6	14066.7	C12RCC$_{1.5\text{-}0.00}$
12.0	18666.7	C13RCC$_{1.5\text{-}0.33}$
62.2	27033.3	C14RCC$_{1.5\text{-}0.67}$
93.6	32266.7	C15RCC$_{1.5\text{-}1.00}$

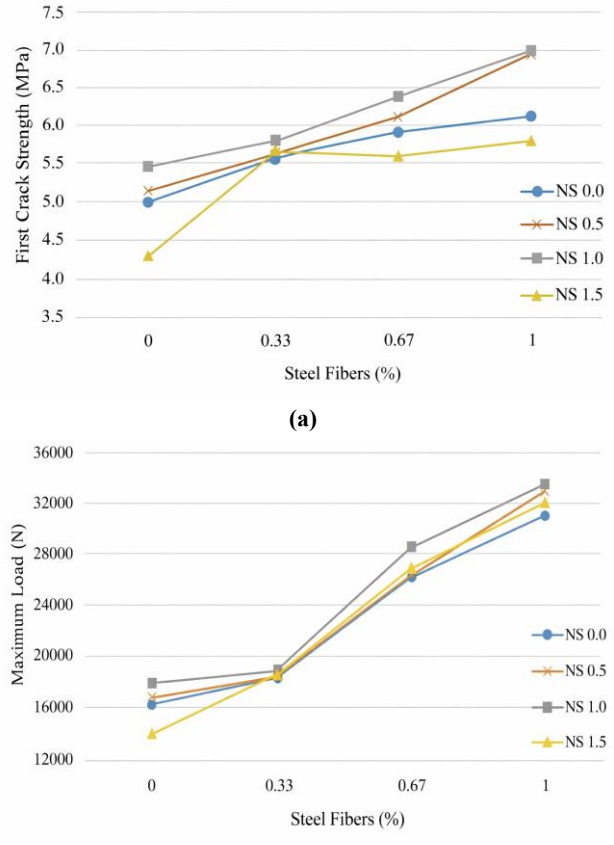

Fig. 12: Comparison of A: First-Crack Strength and B: Maximum Load in 28-Day RCC Composites

The maximum load of RCC increases with the addition of steel fibers and nano-silica. In fiber-reinforced mixes without nano-silica, maximum load rises by 10.2%–87.2% as fiber content increases from 0.33% to 1.0%. In mixes containing 0.5%–1.5% nano-silica, combined increases in fiber and nano-silica content further enhance maximum load, with gains up to 102.6%.

8. Comparison of the parameters of the two-parameter Weibull distribution for fatigue-life data calculated with the results of other researchers

The values of the two-parameter Weibull distribution parameters calculated in this study for pure RCC and composite RCC containing steel fibers, also nano-silica particles have been compared with the values calculated by other researchers.

The two-parameter Weibull distribution parameters obtained by Mohammadi for pure conventional concrete at stress levels of 0.85, 0.80, and 0.70 are presented in Table 12, and for fiber-reinforced concrete containing 1% steel fibers with a length of 50 mm at stress levels of 0.85, 0.80, and 0.70 in Table 13 [43]. The two-parameter Weibull distribution parameters calculated by Oh for pure conventional concrete at stress levels of 0.85, 0.75, and 0.65 are shown in Table 14 [24, 30]. Additionally, the two-parameter Weibull distribution parameters calculated by Singh for fiber-reinforced concrete containing 1% steel fibers at stress levels of 0.90, 0.85, 0.80, and 0.75 are presented in Table 15 [44].

The two-parameter Weibull distribution parameters obtained in this study for the pure roller compacted concretes P2RCC, P3RCC, P4RCC, and P5RCC, as presented in Table 16 , have been compared with the values calculated by Mohammadi and Oh in Figure 13.

Table 13: Parameters of the two-parameter Weibull distribution of ordinary pure concrete calculated by Mohammadi [43].

	Estimated Parameters	Stress Level (S)		
		0.85	0.8	0.7
Mohammadi (Plain Concrete)	α	3.5457	2.7782	2.2393
	u	1749	9229	104638

Table 14: Parameters of the two-parameter Weibull distribution of ordinary pure concrete calculated by Oh [30].

	Estimated Parameters	Stress Level (S)		
		0.85	0.75	0.65
Oh (Plain Concrete)	α	3.9	2.4	2.2

Table 15: Parameters of the two-parameter Weibull distribution of fiber-reinforced concrete calculated by Singh [44].

	Estimated Parameters	Stress Level (S)			
		0.9	0.85	0.8	0.75
S. P. Sing (Fibrous Concrete 1%)	α	2.1682	1.3821	1.2385	1.1249
	u	1312	19.8350	174.1950	972.447

Table 16: Parameters of the two-parameter Weibull distribution for fatigue life data at different stress levels of pure roller compacted concrete samples and roller compacted concrete composites.

	Estimated Parameter	Stress Level (S)		
		0.95	0.9	0.85
P2RCC	α	3.5604	3.2977	2.6984
	u	10.0070	44.6748	181.2633
P3RCC	α	2.9025	2.7488	2.1846
	u	12.6346	61.7191	218.3955
P4RCC	α	2.6652	2.5995	2.0966
	u	17.3221	78.2161	335.1865
P5RCC	α	2.4110	2.3654	1.9510
	u	24.8057	129.7566	408.6286
$C1RCC_{0.0\text{-}0.33}$	α	3.5107	٣.٢٢٧٧	2.4985
	u	16.9035	79.8739	333.4267
$C2RCC_{0.0\text{-}0.67}$	α	3.3075	2.9088	2.1455
	u	31.8245	155.6032	664.6716
$C3RCC_{0.0\text{-}1.00}$	α	2.9663	2.7174	2.0437
	u	60.6211	227.1505	1134.8370
$C4RCC_{0.5\text{-}0.00}$	α	3.6773	3.4483	2.5767
	u	14.5544	51.5858	189.5830
$C5RCC_{0.5\text{-}0.33}$	α	3.5475	3.2292	2.4953
	u	19.6910	84.6900	339.9617
$C6RCC_{0.5\text{-}0.67}$	α	3.1041	2.7887	1.9277
	u	41.7468	165.3350	669.4289
$C7RCC_{0.5\text{-}1.00}$	α	3.0581	2.7031	1.8256
	u	68.4529	236.7814	1245.1590
$C8RCC_{1.0\text{-}0.00}$	α	3.8654	3.6026	2.6292
	u	11.6465	61.3409	371.0542
$C9RCC_{1.0\text{-}0.33}$	α	3.5966	3.2099	2.2214
	u	27.4467	108.0530	370.5319
$C10RCC_{1.0\text{-}0.67}$	α	3.2764	3.1161	2.1320
	u	48.3899	170.0025	898.7989
$C11RCC_{1.0\text{-}1.00}$	α	2.9624	2.8510	1.9943
	u	76.3664	296.1602	1696.7350

Additionally, the distribution parameters of the samples C3RCC0.0 and C3RCC1.00 obtained in this research, which are presented in Table 17, have been compared with the values calculated by Mohammadi and Singh for fiber-reinforced concrete in Figure 14.

Table 17: Parameters of the Two-Parameter Weibull Distribution of Fiber-Reinforced Concrete Calculated by Mohammadi [43].

	Estimated Parameters	Stress Level (S)		
Mohammadi (Fibrous Concrete 1%)		0.9	0.85	0.8
	α	2.366	1.811	1.7039
	u	1593	13699	84177

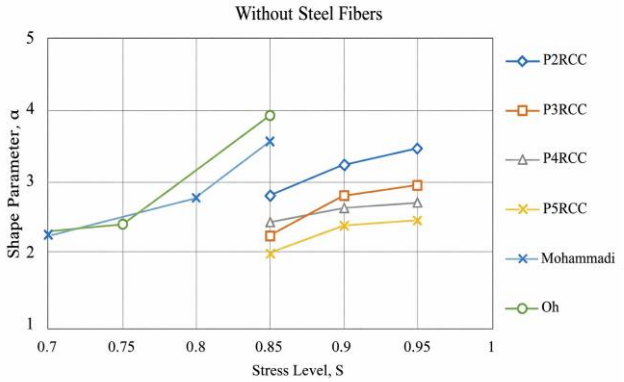

Fig. 13: Comparison of the distribution shape parameters of the two-parameter Weibull for plain RCC and plain conventional concrete

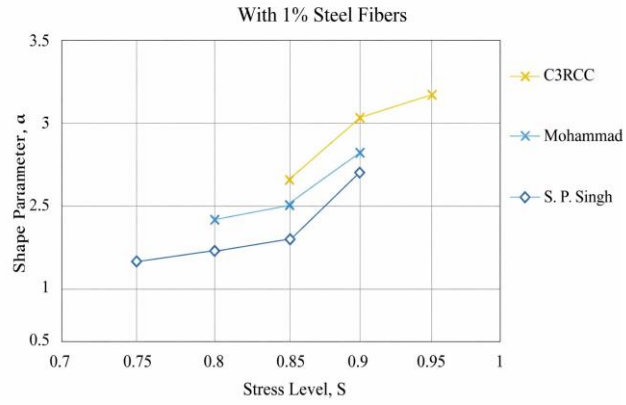

Fig. 14: Comparison of the Weibull distribution parameters of fiber-reinforced roller concrete and conventional fiber-reinforced concrete

According to Figures 13 and 14, there is a similar trend in the values of the parameters of the two-parameter Weibull distribution calculated in this study for plain concrete, pure roller concrete, fiber concrete, and fiber roller concrete, compared to the values calculated by other researchers.

8.1 S–N Relationship

Fatigue performance is commonly represented through an S–N curve, which describes the association between the maximum fatigue stress (S), expressed either as a percentage of the ultimate static flexural capacity or as the actual applied peak fatigue stress, and the corresponding number of cycles to failure (N). To establish a comparative correlation between stress level and fatigue life, each dataset was fitted using linear regression and the resulting trends were plotted. The S–N curves for plain RCC and for the composite RCC mixtures reinforced with steel fibers and nano-silica, incorporated at volumetric fractions of 0.33%, 0.67%, and 1%, and at weight ratios of 0.5%, 1%, and 1.5%, are presented in Figures 15 and 16.

According to the results illustrated in Figures 15 and 16, both plain RCC specimens and RCC-based composites exhibit a clear trend: as the applied stress level increases, the number of cycles to failure decreases. For plain RCC, at a given stress level, specimens with higher compressive strength endure a greater number of load cycles before failure.

In RCC composites without nano-silica, increasing the steel-fiber content leads to a longer fatigue life. A similar trend is observed in composites containing 0.5% and 1% nano-silica, where a higher dosage of steel fibers results in more cycles to failure. In mixtures without steel fibers, raising the nano-silica content also enhances the fatigue life. Furthermore, in composites containing 0.33%, 0.67%, and 1% steel fibers, increasing nano-silica similarly extends the number of cycles to failure. Overall, the beneficial effect of steel fibers on improving fatigue resistance is greater than that provided by nano-silica

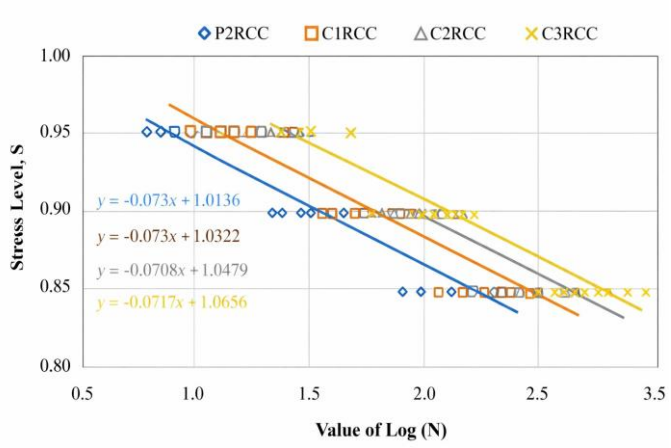

Fig. 15: Comparison of S–N Relationships for the RCC Composites C3RCC$_{0.0\text{-}1.00}$, C2RCC$_{0.0\text{-}0.67}$, C1RCC$_{0}$.0-0.33, and P2RCC

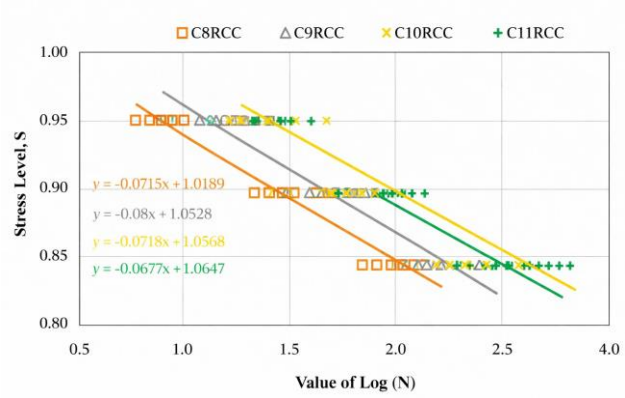

Fig. 16: Comparative S–N Curves for RCC Composites $C11RCC_{1.0\text{-}1.00}$, $C10RCC_{1.0\text{-}0.67}$, $C9RCC_{1.0\text{-}0.33}$, and $C8RCC_{1.0\text{-}0.00}$

9. Conclusion

The flexural fatigue behavior of RCC shows that at high stress levels, failure occurs immediately after the first visible crack, while at lower stress levels, specimens withstand additional cycles despite initial cracking. In composite RCC, failure results from a combination of fiber pullout and fiber fracture. The two-parameter Weibull distribution was found suitable for modeling fatigue-life data at stress levels of 0.95, 0.90, and 0.85 for both plain and composite RCC. The shape parameter (α) and life characteristic (u) were determined using graphical, moment-based, and maximum likelihood methods, all yielding comparable outcomes. The shape parameter increases with stress level, indicating reduced variability of fatigue life under higher stresses and greater scatter at lower stresses. For plain RCC, higher compressive strength corresponds to lower shape parameters. In composite RCC without nano-silica, increasing steel fiber content decreases the shape parameter, reflecting greater variability in fatigue life. In mixes containing 0.5% and 1% nano-silica, a similar decreasing trend with higher fiber content is observed. Conversely, in fiber-free mixes, increasing nano-silica content raises the shape parameter. In mixtures containing 0.33%, 0.67%, and 1% steel fibers, higher nano-silica content also leads to increased shape parameters.

In both plain RCC specimens and RCC composites without steel fibers, the residual strength indices $R_{5,10}$ and $R_{10,20}$ are equal to zero. In RCC mixtures without nano-silica, increasing the steel-fiber content leads to higher residual strength indices. Specifically, when the fiber volume fraction rises from 0.33% to 1.00%, the values of $R_{5,10}$ and $R_{10,20}$ show a clear increase. A similar trend is observed in RCC composites containing 0.5%, 1.0%, and 1.5% nano-silica, where raising the steel-fiber content from 0.33% to 1.00% also enhances the residual strength indices. The greatest improvement in these indices is associated with the specimen designated $C11RCC_{1.0\text{-}1.00}$.

References

[1] Maitra, S. R., Reddy, K. S., & Ramachandra, L. S. (2020). Material and size effect on fatigue damage of concrete for pavement application. *Transportation Research Procedia*, *48*, 3717-3724. https://doi.org/10.1016/j.trpro.2020.08.071

[2] Celik, K., Meral, C., Mancio, M., Mehta, P. K., & Monteiro, P. J. (2014). A comparative study of self-consolidating concretes incorporating high-volume natural pozzolan or high-volume fly ash. *Construction and Building materials*, *67*, 14-19. https://doi.org/10.1016/j.conbuildmat.2013.11.065

[3] Zerbino, R., Giaccio, G., & Isaia, G. C. (2011). Concrete incorporating rice-husk ash without processing. *Construction and building materials*, *25*(1), 371-378. https://doi.org/10.1016/j.conbuildmat.2010.06.016

[4] Liew, K. M., Sojobi, A. O., & Zhang, L. W. (2017). Green concrete: Prospects and challenges. *Construction and building materials*, *156*, 1063-1095. https://doi.org/10.1016/j.conbuildmat.2017.09.008

[5] Güneyisi, E. (2010). Fresh properties of self-compacting rubberized concrete incorporated with fly ash. *Materials and structures*, *43*(8), 1037-1048. https://doi.org/10.1617/s11527-009-9564-1

[6] Naik, T. R., Kumar, R., Ramme, B. W., & Canpolat, F. (2012). Development of high-strength, economical self-consolidating concrete. *Construction and Building Materials*, *30*, 463-469. https://doi.org/10.1016/j.conbuildmat.2011.12.025

[7] Khalid, M. Q., & Abbas, Z. K. (2023). Recycled concrete aggregated for the use in roller compacted concrete: A literature review. *Journal of Engineering*, *29*(03), 142-153. https://doi.org/10.31026/j.eng.2023.03.10

[8] Slattery, K. (2014). Global developments in the aggregate industry. *Global Aggregates Information, Network*.

[9] ACI 325.10R-95. (1995). *Report on RCC Pavements.*

[10] Chhorn, C., Hong, S. J., & Lee, S. W. (2018). Relationship between compressive and tensile strengths of roller-compacted concrete. *Journal of Traffic and Transportation Engineering (English Edition)*, *5*(3), 215-223. https://doi.org/10.1016/j.jtte.2017.09.002

[11] Reddy, A. N., & Meena, T. (2017). A comprehensive overview on performance of nano silica concrete. *International Journal of pharmacy &Technology. ISSN*, *2017*, 5518-29.

[12] Paryad, P., Naderpour, H., & Sharbatdar, M. K. (2025). Influence of Steel Fiber Characteristics on Mechanical Behavior of Roller-Compacted Concrete Pavement. *Journal of Structural Design and Construction Practice*, *30*(2), 04025016. https://doi.org/10.1061/JSDCCC.SCENG-1667

[13] Mohanty, A., Biswal, D. R., Pradhan, S. K., & Mohanty, M. (2025). Impact of Nanomaterials on the Mechanical Strength and Durability of Pavement Quality Concrete: A Comprehensive Review. *Eng*, *6*(4), 66. https://doi.org/10.3390/eng6040066

[14] Swilam, E., Saad, M. A., M Morsi, A., & Eisa, M. S. (2024). Evaluation the performance of Rigid Pavement Modified with admixture of Nano Silica and Glass Fiber: A

review. *Benha Journal of Applied Sciences*, *9*(5), 113-126. https://doi.org/10.21608/bjas.2024.280651.1403

[15] Seifollahi, F., & Mohammadi, Y. (2022). Experimental Study of Mechanical Properties and Relationships between Strengths of Pure and Nanosilica-Steel fiber-contained Roller Compacted Concrete at Different Curing Days.

[16] ACI 544.1R-96., (2002). *Report on Fiber Reinforced Concrete.*

[17] Kavussi, A., & Modarres, A. (2010). Laboratory fatigue models for recycled mixes with bitumen emulsion and cement. *Construction and building materials*, *24*(10), 1920-1927. https://doi.org/10.1016/j.conbuildmat.2010.04.009

[18] Gao, D., Gu, Z., Zhu, H., & Huang, Y. (2020, October). Fatigue behavior assessment for steel fiber reinforced concrete beams through experiment and fatigue prediction model. In *Structures,* 27, 1105-1117. https://doi.org/10.1016/j.istruc.2020.07.028

[19] Lv, Y., Cheng, H. M., & Ma, Z. G. (2012). Fatigue performances of glass fiber reinforced concrete in flexure. *Procedia Engineering*, *31*, 550-556. https://doi.org/10.1016/j.proeng.2012.01.1066

[20] Jaeckel, H. R., & Swanson, S. R. (1968). *Random Load Spectrum Test to Determine Durability of Structural Components of Automotive Vehicles*. L'Organització.

[21] ASTM International., American Society for Testing and Materials., & American Society for Testing and Materials. (1963). *A guide for fatigue testing and the statistical analysis of fatigue data*. West Conshohocken, Pa.: ASTM International.

[22] Gumbel, E. J. (1963). Parameters in the distribution of fatigue life. *Journal of the Engineering Mechanics Division*, *89*(5), 45-64. https://doi.org/10.1061/JMCEA3.0000418

[23] Madayag, A. F. (1969). *Metal Fatigue: Theory and Design.*

[24] Oh, B. H. (1986). Fatigue analysis of plain concrete in flexure. *Journal of Structural Engineering*, *112*(2), 273-288. https://doi.org/10.1061/(ASCE)07339445(1986)112:2(273)

[25] Asce. (1982). Committee on fatigue and fracture reliability of the committee on structural safety and reliability of the structural division. Fatigue reliability 1–4. *J. Struct. Div.*, *108*(ST1), 3-88.

[26] Henley, E. J. (1984). Probabilistic engineering design: principles and applications by James N. Siddall. *Chemical Engineering Education*, *18*(3), 144-145.

[27] Kennedy, J. B. (1986). *Basic statistical methods for engineers and scientists.*

[28] Barlow, R.E., F. Proschan. (1996). Mathematical theory of reliability. *Society for Industrial and Applied Mathematics*.

[29] Wirsching, P. H., & Yao, J. T. (1970). Statistical methods in structural fatigue. *Journal of the Structural Division*, *96*(6), 1201-1219. https://doi.org/10.1061/JSDEAG.0002603

[30] Oh, B. H. (1991). Cumulative damage theory of concrete under variable-amplitude fatigue loadings. *Materials Journal*, *88*(1), 41-48.

[31] Benjamin, J. R., & Cornell, C. A. (2014). *Probability, statistics, and decision for civil engineers*. Courier Corporation.

[32] Model Code (2010, 2012). *Final draft. FIB Bulletin, EPFL Lausanne.*

[33] ASTM C595-08a. (2008). *Standard Specification for Blended Hydraulic Cements.*

[34] ASTM D1129. (2020). *Standard Terminology Relating to Water.*

[35] ASTM C136-06. (2015). *Standard Test Method for Sieve Analysis of Fine and Coarse Aggregates.*

[36] ASTM C29/C29M-97. (2017). *Standard Test Method for Bulk Density ("Unit Weight") and Voids in Aggregate.*

[37] ACI 211.1-91. (2002). *Standard Practice for Selecting Proportions for Normal, Heavyweight, and Mass Concrete.*

[38] AASHTO M 6. (2013). *Standard Specification for Fine Aggregate for Hydraulic Cement.*

[39] ASTM C1176-92. (2017). *Standard Practice for Making Roller-Compacted Concrete in Cylinder Molds Using a Vibrating Table.*

[40] ASTM C1435-99. (2017). *Standard Practice for Molding Roller-Compacted Concrete in Cylinder Molds Using a Vibrating Hammer.*

[41] ACI 211.3R-02. (2009). *Guide for Selecting Proportions for No-Slump Concrete.*

[42] ASTM C192/C192M-15. (2016). *Standard Practice for Making and Curing Concrete Test Specimens in the Laboratory.*

[43] Mohammadi, Y. A. G. H. O. U. B. (2002). Behaviour of steel fibre reinforced concrete in flexural fatigue. *India: University of Roorkee*.

[44] Singh, S. P., & Kaushik, S. K. (2000). Flexural fatigue life distributions and failure probability of steel fibrous concrete. *Materials Journal*, *97*(6), 658-667.